High-Order CESE Methods for the Euler Equations

David L. Bilyeu,* Yung-Yu Chen, † and S.-T. John Yu ‡
The Ohio State University, Columbus, OH 43210, USA

Recently, Chang[1] reported a new class of high-order CESE methods for solving nonlinear hyperbolic partial differential equations. A series of high-order algorithms have been developed based on a systematic, recursive formulation that achieves fourth-, sixth-, and eighth-order accuracy. The new high-order CESE method shares many favorable attributes of the original second- order CESE method, including: (i) compact mesh stencil involving only the immediate mesh nodes surrounding the node where the solution is sought, (ii) the CFL stability constraint remains to be the same, i.e., ≤ 1, as compared to the original second-order method, and (iii) superb shock capturing capability without using an approximate Riemann solver. The new algorithm has been demonstrated by solving Burger's equation.

In the present paper, we extend Chang's high-order method for system of linear and nonlinear hyperbolic partial differential equations. A general formulation is presented for solving the coupled equations with arbitrarily high-order accuracy. To demonstrate the formulation, several linear and nonlinear cases are reported. First, we solve a convection equation with source term and the linear acoustics equations. We then solve the Euler equations for acoustic waves, a blast wave, and Shu and Osher's test case for acoustic waves interacting with a shock. Numerical results show higher-order convergence by continuous mesh refinement.

I. Introduction

In this work, we extend Chang's fourth-order CESE method[1] for one nonlinear hyperbolic equation to a system of coupled hyperbolic partial differential equations (PDEs). The new formulation is general and can be used to achieve arbitrarily order of convergence. To demonstrate the capabilities of the new scheme, we apply the method to solve three sets of equations: (i) the one-dimensional Euler equations, (ii) the linearized acoustic equations, and (iii) a convection equation with a source term.

The original second-order CESE method[2] solves the hyperbolic PDEs by discretizing the space-time domain by using the conservation elements (CEs) and solution elements (SEs). The profiles of unknowns are prescribed by assumed discretization inside SEs. Aided by the approximation for the unknowns in the SEs, space-time flux conservation can be enforced over each CE. The calculation of space-time flux conservation results in the formulation for updating the unknowns in the time marching process. The special features of the CESE method include: (i) The *a* scheme, the core scheme of the CESE method, is non-dissipative. (ii) The CESE method has the most compact mesh stencil and it involves only the immediate neighboring mesh points that surround the mesh node where the solution is sought. (iii) The method uses explicit integration in time marching. The stability criterion is CFL ≤ 1. (iv) No approximate Riemann solver is used and the scheme is simple and efficient.

This paper is organized as the following. Section II reports the fourth-order CESE method for the coupled equations formulated in a vector form. Section III shows the application of the general formulation to the one-dimensional Euler, linear acoustic, and convection equation. Section IV provides the results and discussions. In Section V, we draw our conclusions.

*Ph.D. Student, Dept. of Mechanical Engineering, bilyeu.4@osu.edu, and AIAA Student Member.
†Ph.D. Candidate, Dept. of Mechanical Engineering, chen.1352@osu.edu.
‡Associate Professor, Dept. of Mechanical Engineering, yu.274@osu.edu and AIAA Member.

II. Arbitrary-Order, One-Dimensional CESE Method

Consider a system of coupled convection equations:

$$\frac{\partial \mathbf{U}}{\partial t} + \frac{\partial \mathbf{F}}{\partial x} = \mathbf{S}, \tag{1}$$

where

$$\mathbf{U} \overset{\text{def}}{=} (u_1, u_2, u_3, \cdots, u_M)^T,$$
$$\mathbf{F} \overset{\text{def}}{=} (f_1, f_2, f_3, \cdots, f_M)^T,$$
$$\mathbf{S} \overset{\text{def}}{=} (s_1, s_2, s_3, \cdots, s_M)^T,$$

There are M equations to be solved in the system Eq. (1).

The space-time stencil used in this derivation is the same as that reported by Chang[3] and is repeated here for completeness. In Fig. (1) the solid dots A, C, and E are the solution points. A is at (x_j, t^n) and C and E are at $(x_{j-1/2}, t^{n-1/2})$ and $(x_{j+1/2}, t^{n-1/2})$, respectively. P^+ is between M^+ and F. P^- is between M^- and B. The distance between $P^\pm$ and $M^\pm$ is determined by a parameter τ. The rectangles $ABCD$ and $ADEF$ are basic CEs (BCEs), while the rectangle $BCEF$ is the compound CE (CCE) associated with the solution point A.

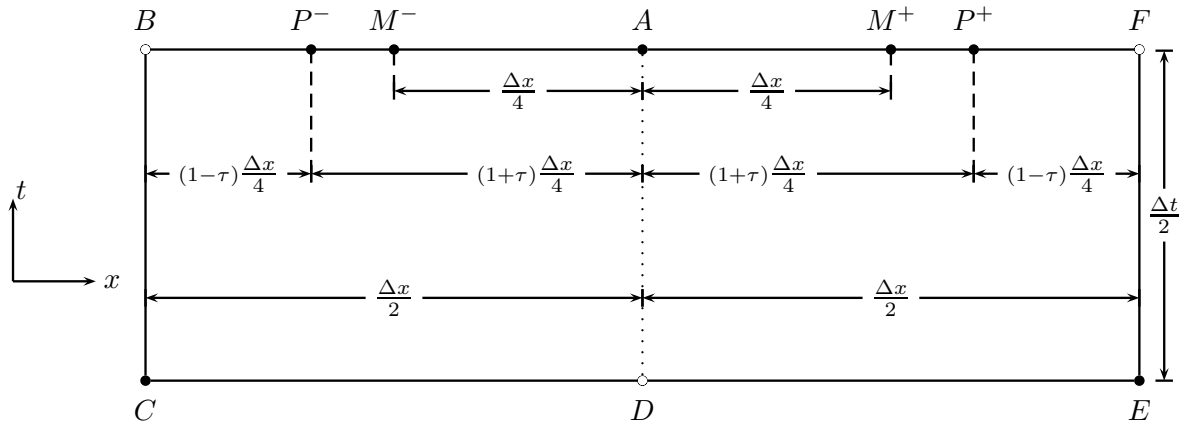

Fig. 1: Mesh nodes in the one-dimensional CESE methods.

To facilitate the discussion, we let SE(j, n) denotes the SE located at $x = x_j$ and $t = t^n$. To denote high-order derivatives, we use the following notations:

$$u_{mx^a t^b} = \frac{\partial^{a+b} u_m}{\partial x^a t^b}$$

In SE(j, n), the unknown variables u_m, $m = 1, \ldots, M$, are approximated by a Taylor series:

$$u_m^*(x, t; j, n) \overset{\text{def}}{=} \sum_{a=0}^{N_M} \sum_{b=0}^{N_M - a} \frac{(u_{mx^a t^b})_j^n}{a!b!} (x - x_j)^a (t - t^n)^b, \tag{2}$$

where N_M is the desired order subtracted by 1, e.g., for the fourth-order scheme, $N_M = 3$. The superscript $*$ represents the numerical approximation of the variable. Inside of a SE $u_{mx^a t^b}$ are constant. The flux functions f_m, $m = 1, \ldots, M$, can also be represented with the Taylor expansion as:

$$f_m^*(x, t; j, n) \overset{\text{def}}{=} \sum_{a=0}^{N_M} \sum_{b=0}^{N_M - a} \frac{(f_{mx^a t^b})_j^n}{a!b!} (x - x_j)^a (t - t^n)^b. \tag{3}$$

Inside a SE, $f_{mx^at^b}$ are constant. An advantage of a Taylor series is that its derivatives can also be expressed as a Taylor series

$$u^*_{mx^zt^i}(x,t;j,n) = \sum_{a=0}^{A}\sum_{b=0}^{B-a} \frac{(u_{mx^{a+z}t^{b+i}})^n_j}{a!b!}(x-x_j)^a(t-t^n)^b \; ; \; \substack{A=N_M-z \\ B=N_M-z-i} \tag{4}$$

and

$$f^*_{mx^zt^i}(x,t;j,n) = \sum_{a=0}^{A}\sum_{b=0}^{B-a} \frac{(f_{mx^{a+z}t^{b+i}})^n_j}{a!b!}(x-x_j)^a(t-t^n)^b \; ; \; \substack{A=N_M-z \\ B=N_M-z-i}. \tag{5}$$

Equations 2 and 3 contain $2\sum_{n=1}^{N_M+1} n$ unknowns. In the following derivation, it will be shown, for a given SE(j,n), the only independent variables are the spatial derivatives $(u_m)^n_j$, $(u_{mx})^n_j$, ..., $(u_{mx^a})^n_j$, $m = 1,\ldots,M$, $a = N_M$. Since it is assumed that the fluxes are known functions of the flow variables. The flux terms in Eq. (3) can be determined from the chain rule. To proceed, we define:

$$f_{m_l} \stackrel{\text{def}}{=} \frac{\partial f_m}{\partial u_l}, \quad f_{m_{l,k}} \stackrel{\text{def}}{=} \frac{\partial^2 f_m}{\partial u_l \partial u_k}, \quad f_{m_{l,k,p}} \stackrel{\text{def}}{=} \frac{\partial^3 f_m}{\partial u_l \partial u_k \partial u_p}, \ldots \tag{6}$$

where $m,l,k,p = 1,\ldots,M$. For SE(j,n), we obtain:

$$\begin{aligned}
\frac{\partial f_m}{\partial y_1} &= \sum_{l}^{Neq} \frac{\partial f_m}{\partial u_l}\frac{\partial u_l}{\partial y_1}, \quad y_1 = x,t \\
\frac{\partial^2 f_m}{\partial y_1 \partial y_2} &= \sum_{l}^{Neq} \frac{\partial f_m}{\partial u_l}\frac{\partial^2 u_l}{\partial y_1 \partial y_2} + \sum_{l,k}^{Neq} \frac{\partial^2 f_m}{\partial u_l \partial u_k}\frac{\partial u_l}{\partial y_1}\frac{\partial u_k}{\partial y_2} \quad (y_1,y_2) = (x,x),(t,t),(x,t) \\
\frac{\partial^3 f_m}{\partial y_1 \partial y_2 \partial y_3} &= \sum_{l}^{Neq} \frac{\partial f_m}{\partial u_l}\frac{\partial^3 u_l}{\partial y_1 \partial y_2 \partial y_3} + \sum_{l,k}^{Neq} \frac{\partial^2 f_m}{\partial u_l \partial u_k}\left(\frac{\partial^2 u_l}{\partial y_1 \partial y_2}\frac{\partial u_k}{\partial y_3} + \frac{\partial^2 u_l}{\partial y_1 \partial y_3}\frac{\partial u_k}{\partial y_2} + \frac{\partial^2 u_l}{\partial y_2 \partial y_3}\frac{\partial u_k}{\partial y_1}\right) \\
&\quad + \sum_{l,k,p}^{Neq} \frac{\partial^3 f_m}{\partial u_l \partial u_k \partial u_p}\frac{\partial u_l}{\partial y_1}\frac{\partial u_k}{\partial y_2}\frac{\partial u_p}{\partial y_3} \quad (y_1,y_2,y_3) = \begin{matrix}(x,x,x), & (t,t,t), \\ (x,x,t), & (x,t,t),\end{matrix}
\end{aligned} \tag{7}$$

for $m = 1,\ldots,M$. Equation Eq. (7) shows the derivatives required by the fourth order scheme but these equations will continue to the derivatives required by the desired order.

By substituting Eqs. (2) and (3) into Eq. (1) in a given SE(j,n), we demand:

$$\frac{\partial u^*_m(x,t;j,n)}{\partial t} + \frac{\partial f^*_m(x,t;j,n)}{\partial x} = s_m, \quad m = 1,\ldots,M. \tag{8}$$

Then by taking derivatives of Eq. (8) in both space and time we get

$$(u^*_{mt})^n_j = (s_m)^n_j - (f^*_{mx})^n_j, \quad (u^*_{mxt})^n_j = (s_{m_x})^n_j - (f^*_{mxx})^n_j, \quad (u^*_{mtt})^n_j = (s_{m_t})^n_j - (f^*_{mxt})^n_j, \ldots.$$

This result can be written in a more general form as

$$u^*_{mx^zt^i} = s^*_{mx^zt^{i-1}} - f^*_{mx^{z+1}t^{i-1}} \tag{9}$$

for $m = 1,\ldots,M$, $z = 0,\ldots N_M$, $i = 1,\ldots N_M - z$. As shown in Eqs. (7) and (9), the only independent variables are the spatial derivatives for each governing equation. As such, there are $(N_M+1)M$ unknowns for M equations associated with a mesh point. For example, a fourth-order representation of the Euler equation would contain 4 unknowns per equation, giving a total of 12 unknowns for the one-dimensional Euler equations.

To proceed, for each of $m = 1,\ldots,M$, the unknowns are categorized as: (i) even-order derivatives, $(u_m)^n_j$, $(u_{mxx})^n_j$, ..., $u_{mx^{2n}}$ and (ii) odd-order derivatives, $(u_{mx})^n_j$, $(u_{mxxx})^n_j$, ... $u_{mx^{2n+1}}$ $n = (OD-1)/2$. In what follows, we introduce an arbitrary order CESE c-τ scheme for a system of M PDEs. The c-τ scheme uses space-time integration for the advancing formula for the even-order derivatives, while the odd-order derivatives are calculated from a central-difference-like procedure.

II.A. Even-Order Derivatives

It can be shown that by differentiating Eq. (8) twice with respect to x, we obtain:

$$\frac{\partial u^*_{mxx}(x,t;j,n)}{\partial t} + \frac{\partial f^*_{mxx}(x,t;j,n)}{\partial x} = \frac{\partial^2 s^*_m}{\partial x^2}, \quad m = 1,\ldots,M, \tag{10}$$

or in a more general form

$$\frac{\partial u^*_{mx^{2z}}(x,t;j,n)}{\partial t} + \frac{\partial f^*_{mx^{2z}}(x,t;j,n)}{\partial x} = \frac{\partial^{2z} s^*_m}{\partial x^{2z}}, \quad z = 0,1,\ldots,(N_M-1)/2. \tag{11}$$

Consider the Euclidean space $\mathcal{E}^2$ with the coordinates $(\xi_1,\xi_2) = (x,t)$. Aided by defining:

$$\mathbf{h}^*_{mx^{2z}} \stackrel{\text{def}}{=} (f^*_{mx^{2z}}(x,t;j,n), u^*_{mx^{2z}}(x,t;j,n))^T, \quad z = 1,\ldots,(N_M-1)/2,$$

and the divergence theorem, Eqs. (8) and (11) can be transformed into integral equations as:

$$\oint_{S(V)} \mathbf{h}^*_{mx^{2z}} \cdot d\mathbf{s} = s^*_{mx^{2z}}, \quad z = 0,\ldots,(N_M-1)/2, \tag{12}$$

where $S(V)$ is the closed boundary of an arbitrary region V and $d\mathbf{s}$ is defined in Fig. (2).

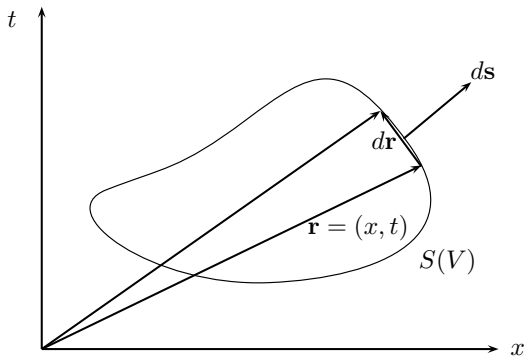

Fig. 2: Space-time integration over an arbitrary closed domain V.

We define:

$$u^*_{m\bar{x}^z\bar{t}^k} \stackrel{\text{def}}{=} \frac{\partial^{z+k} u^*_m}{\partial x^z t^k} \left(\frac{\Delta x}{4}\right)^z \left(\frac{\Delta t}{4}\right)^k \tag{13}$$

$$f^*_{m\bar{x}^z\bar{t}^k} \stackrel{\text{def}}{=} \frac{\partial^{z+k} f^*_m}{\partial x^z t^k} \left(\frac{\Delta x}{4}\right)^z \left(\frac{\Delta t}{4}\right)^k \tag{14}$$

$$s_{m\bar{x}^z\bar{t}^k} \stackrel{\text{def}}{=} \frac{\partial^{z+k} s_m}{\partial x^z t^k} \left(\frac{\Delta x}{4}\right)^z \left(\frac{\Delta t}{4}\right)^k \tag{15}$$

where $\Delta x = x_{j+1/2} - x_{j-1/2}$ and $\Delta t = t^n - t^{n-1}$. In order to write equations more compactly, any local constant enclosed within a square bracket will be evaluated at the location specified by the subscript and superscript written on the enclosing square bracket, e.g.:

$$(u_{mxx})^n_j + (u_{mxxx})^n_j \frac{\Delta x}{2} + (u_{mxxt})^n_j \frac{\Delta t}{2} \equiv \left[u_{mxx} + u_{mxxx}\frac{\Delta x}{2} + u_{mxxt}\frac{\Delta t}{2}\right]^n_j.$$

Aided by Eqs. (13) and (14), Eq. (12) gives:

$$(u_{m\bar{x}^z})_j^n = \frac{1}{\Delta x}\iint s_{m\bar{x}^z}dV + \frac{1}{2}\sum_{k=0}^{N_M-z}\frac{2^k}{(k+1)!}\left(\left[u_{m\bar{x}^{k+z}} + \frac{\Delta t}{\Delta x}f_{m\bar{x}^z\bar{t}^{z+k}}\right]_{j-1/2}^{n-1/2} + \left[(-1)^i u_{m\bar{x}^{k+z}} - \frac{\Delta t}{\Delta x}f_{m\bar{x}^z\bar{t}^{z+k}}\right]_{j+1/2}^{n-1/2}\right) - \sum_{k=1}^{\frac{N_M-z-1}{2}}\frac{2^{2k}}{(2k+1)!}(u_{m\bar{x}^{2k+z}})_j^n \quad (16)$$

Equation (16) provides and explicit formulation for all even spatial derivatives. As long as the highest even derivative is calculated first the last term on the RHS will have already been calculated. It should also be noted that the $*$ is absent from the source term. This is because the source term treatment varies when dealing with different flow physics.

II.B. Odd-Order Derivatives

In order to compute the odd derivatives a central differencing approach is applied following the c-τ scheme. There are two possible formulations for the odd-order derivatives (i) the standard c-τ scheme which is applicable if there are no discontinuities present and (ii) a re-weighted c-τ scheme which is used if there are discontinuities in the flow field.

In order to mitigate the dissipation as the local CFL number decreases the central differencing is applied at points P^+ and P^-. Where $P^\pm$ are points located at

$$x\left(P^+\right) = x_j + (1+\tau)\frac{\Delta x}{4} = x_{j+1/2} - (1-\tau)\frac{\Delta x}{4}, \quad (17)$$

$$x\left(P^-\right) = x_j - (1+\tau)\frac{\Delta x}{4} = x_{j-1/2} + (1-\tau)\frac{\Delta x}{4}. \quad (18)$$

Where τ is the absolute value of the local CFL number.

First we define $u^*_{m\bar{x}^z}(P^\pm)$ to be the Taylor series expansion of $(u_{m\bar{x}^z})_n^j$ from (x_j, t^n) to $x(P^\pm)$. Then we can solve for $u_{m\bar{x}^{z+1}}$ by subtracting $u^*_{m\bar{x}^z}(P^-)$ from $u^*_{m\bar{x}^z}(P^+)$:

$$u_{m\bar{x}^{z+1}} = \frac{u_{m\bar{x}^z}(P^+) - u_{m\bar{x}^z}(P^-)}{2(1+\tau)} - \sum_{k=1}^{\frac{N_M-1-z}{2}}\frac{1}{(2k+1)!}u_{m\bar{x}^{2k+1+z}}(1+\tau)^{2k}, \quad (19)$$

for $z = 0, 2, 4, \ldots, N_M - 1$ and $m = 1, 2, \ldots, M$. Since we can not calculate $u^*_{m\bar{x}^z}(P^\pm)$ we approximate it by $u'_{m\bar{x}^z}(P^\pm)$. Where $u'_{m\bar{x}^z}(P^\pm)$ is the Taylor series expansion from $(x_{j\pm1/2,t^{n-1/2}})$ to $x(P^\pm)$ respectively.

$$u_{m\bar{x}^{z+1}} = \frac{u'_{m\bar{x}^z}(P^+) - u'_{m\bar{x}^z}(P^-)}{2(1+\tau)} - \sum_{k=1}^{\frac{N_M-1-z}{2}}\frac{1}{(2k+1)!}u_{m\bar{x}^{2k+1+z}}(1+\tau)^{2k},$$

When discontinuities are present in the flow field a re-weighting of the derivatives is required. All previously derived re-weighting schemes used in second order CESE schemes should be applicable to the higher order CESE schemes. In this paper the derivation of the W2 scheme[3] will be presented. First the function W is given as

$$W_\pm(x_-, x_+, \alpha) = \frac{|x_\mp|^\alpha}{|x_-|^\alpha + |x_+|^\alpha}. \quad (20)$$

To remain stable in the presence of discontinuities $\alpha \geq 1$. The odd-order derivatives are now defined by:

$$(u_{m\bar{x}^z})_j^n \stackrel{\text{def}}{=} (\omega_{m-})_z\left(\hat{u}_{m\bar{x}^{-z}}\right) + (\omega_{m+})_z\left(\hat{u}_{m\bar{x}^{+z}}\right), \quad (21)$$

where

$$(\omega_{m\pm})_z = W_{\pm}(u^c_{m\bar{x}^{-z}}, u^c_{m\bar{x}^{+z}}, \alpha_z), \tag{22}$$

with

$$\hat{u}_{m\bar{x}^{\mp z}} \stackrel{\text{def}}{=} \pm\frac{(u_{m\bar{x}^{z-1}})^n_j - u'_{mx^{z-1}}(P^{\mp})}{1+\tau},$$

$$u^c_{m\bar{x}^z\mp} \stackrel{\text{def}}{=} \pm\frac{1}{2}((u_{mx^{z-1}})^n_j - (u'_{mx^{z-1}})^n_{j\mp 1/2}),$$

where $(u'_{mx^{z-1}})^n_{j\pm 1/2}$ is the Taylor series expansion from $(x_{j\pm -1/2}, n-1/2)$ to $(x_{j\pm -1/2}, n)$.

The above equations provide an explicit formulation for the odd spatial derivatives when discontinuities are present in the flow field.

III. Jacobian Matrices

In this section we present the derived Jacobian matrices for the different flow physics used as test cases. The three flow physics used are the Euler, linear acoustic, and convection equations.

To construct a fourth-order CESE solver for the one-dimensional Euler equations, we plug the following unknown vector and flux function vector into Eq. (1):

$$\begin{aligned}\mathbf{U} &= (u_1, u_2, u_3)^T = \left(\rho, \rho v, p/(\gamma-1) + \rho v^2/2\right)^T, \\ \mathbf{F} &= \left(\rho v, \rho v^2 + p, (\rho E + p)v\right)^T \\ &= \left(u_2, (\gamma-1)u_3 + 1/2(3-\gamma)u_2^2/u_1, \gamma u_2 u_3/u_1 - 1/2(\gamma-1)u_2^3/u_1^2\right)^T,\end{aligned}$$

where ρ is the density, v is the velocity, E is the internal energy and γ is the ratio of specific heat. For the higher order derivatives the order of differentiation does not mater, i.e. $f_{m_{l,k}} = f_{m_{k,l}}$ and $f_{m_{l,k,p}} = f_{m_{l,p,k}} = f_{m_{k,l,p}} = f_{m_{k,p,l}} = f_{m_{p,l,k}} = f_{m_{p,k,l}}$ so only the first such permutation is expressed. The first-order derivatives of the flux function f_1 are:

$$f_{1_1} = 0, \quad f_{1_2} = 1, \quad f_{1_3} = 0,$$

and the second- and third-order derivatives are:

$$\begin{aligned} f_{1_{l,k}} &= 0, \quad l,k = 1,2,3, \\ f_{1_{l,k,p}} &= 0, \quad l,k,p = 1,2,3.\end{aligned}$$

The first-order derivatives of the flux function f_2 are:

$$f_{2_1} = \frac{1}{2}(\gamma-3)\frac{u_2^2}{u_1^2}, \quad f_{2_2} = (3-\gamma)\frac{u_2}{u_1}, \quad f_{2_3} = \gamma - 1,$$

the second-order derivatives are:

$$\begin{array}{lll} f_{2_{1,1}} = -\frac{u_2^2(\gamma-3)}{u_1^3}, & f_{2_{1,2}} = \frac{(\gamma-3)u_2}{u_1^2}, & f_{2_{1,3}} = 0, \\ f_{2_{2,2}} = \frac{(3-\gamma)}{u_1}, & f_{2_{2,3}} = 0, & f_{2_{3,3}} = 0, \end{array}$$

and the third-order derivatives are:

$$\begin{array}{lll} f_{2_{1,1,1}} = 3\frac{u_2^2(\gamma-3)}{u_1^4}, & f_{2_{1,1,2}} = -2\frac{(\gamma-3)u_2}{u_1^3}, & f_{2_{1,1,3}} = 0, \\ f_{2_{1,2,2}} = \frac{(\gamma-3)}{u_1^2}, & f_{2_{1,2,3}} = 0, & f_{2_{1,3,3}} = 0, \\ f_{2_{2,2,2}} = 0, & f_{2_{2,2,3}} = 0, & f_{2_{3,3,3}} = 0. \end{array}$$

The first-order derivatives of the flux function f_3 are:

$$f_{3_1} = -\frac{\gamma u_2 u_3}{u_1^2} + \frac{(\gamma-1)u_2^3}{u_1^3}, \quad f_{3_2} = \frac{\gamma u_3}{u_1} - \frac{3}{2}(\gamma-1)\frac{u_2^2}{u_1^2}, \quad f_{3_3} = \frac{\gamma u_2}{u_1},$$

the second-order derivatives are:

$$f_{3_{1,1}} = 2\frac{\gamma u_2 u_3}{u_1^3} - 3\frac{(\gamma-1)u_2^3}{u_1^4}, \quad f_{3_{1,2}} = -\frac{\gamma u_3}{u_1^2} + 3\frac{(\gamma-1)u_2^2}{u_1^3}, \quad f_{3_{1,3}} = -\frac{\gamma u_2}{u_1^2},$$
$$f_{3_{2,2}} = -3\frac{(\gamma-1)u_2}{u_1^2}, \quad f_{3_{2,3}} = \frac{\gamma}{u_1}, \quad f_{3_{3,3}} = 0,$$

the third-order derivatives are:

$$f_{3_{1,1,1}} = 12\frac{u_2^3(\gamma-1)}{u_1^5} - 6\frac{\gamma u_2 u_3}{u_1^4}, \quad f_{3_{1,1,2}} = 2\frac{\gamma u_3}{u_1^3} - 9\frac{(\gamma-1)u_2^2}{u_1^4}, \quad f_{3_{1,1,3}} = 2\frac{\gamma u_2}{u_1^3},$$
$$f_{3_{1,2,2}} = 6(\gamma-1)\frac{u_2}{u_1^3}, \quad f_{3_{1,2,3}} = -\frac{\gamma}{u_1^2}, \quad f_{3_{1,3,3}} = 0$$
$$f_{3_{2,2,2}} = -3\frac{\gamma-1}{u_1^2}, \quad f_{3_{2,2,3}} = 0, \quad f_{3_{3,3,3}} = 0.$$

Next we present the derived Jacobian for the linear acoustic equation

$$\mathbf{U} = (u_1, u_2)^T = (\rho, v)^T,$$
$$\mathbf{F} = \left(\rho_{\text{inf}} v, \frac{a_{\text{inf}}^2}{\rho_{\text{inf}}}\rho\right)^T = \left(\rho_{\text{inf}} u_2, \frac{a_{\text{inf}}^2}{\rho_{\text{inf}}}u_1\right)^T$$

The first-order derivatives for the flux functions are:

$$f_{1_1} = 0, f_{1_2} = \rho_{\text{inf}}$$
$$f_{2_1} = \frac{a_{\text{inf}}^2}{\rho_{\text{inf}}}, f_{2_2} = 0.$$

Since all of the first-order derivatives are constant the higher derivatives are zero. This reduces the calculation of all fluxes to a matrix vector multiplication.

Finally we present the derivation needed for the convection with source term equation.

$$\frac{du}{dt} + a\frac{du}{dx} = aS_0\cos(x)$$

where a and S_0 are constant. In this case the source term is only a function of space and an exact integration is possible. For $S = aS_0\cos(x)$ the integrals become

$$\iint S = aS_0\frac{\Delta t}{2}\sin(x)|_{x_{j-1/2}}^{x_{j+1/2}},$$
$$\iint S_{\bar{x}\bar{x}} = -aS_0\left(\frac{\Delta x}{4}\right)^2\frac{\Delta t}{2}\sin(x)|_{x_{j-1/2}}^{x_{j+1/2}} \quad ,\ldots,$$
$$\iint S_{\bar{x}^{2n}} = (-1)^{n/2}aS_0\left(\frac{\Delta x}{4}\right)^{2n}\frac{\Delta t}{2}sin(x)|_{x_{j-1/2}}^{x_{j+1/2}}, \text{ for } n = 0, 1, \ldots, \frac{N_M - 1}{2}.$$

IV. Results

The following test cases show how the CESE method improves as the order of accuracy of the method employed increases. These cases are presented, including (i) acoustic waves modeled by the linearized Euler equations, (ii) acoustic waves modeled by the nonlinear Euler equations, and (iii) a simple convection equation with a source term. For all three cases, we calculate the order of accuracy by using the following formula:

$$\ell^2 \stackrel{\text{def}}{=} \sqrt{\int |\phi|^2 dx} \approx \sqrt{\sum_i |\phi_i|^2 \Delta x_i}$$

where ϕ_i is defined as the difference between the analytical and numerical solution and Δx_i is the grid spacing at a given location i. In all cases Δx is constant. The rate of convergence is taken as the slope of the best fit line through the points ($log_{10}(\Delta x)$, $log_{10}(\ell^2)$).

The first test case is the calculation of acoustic waves by solving the linearized Euler equations. The analytical solution for the linearized acoustic wave equation is

$$\rho = \rho_{\text{inf}} + \frac{\varepsilon \rho_{\text{inf}}}{a_{\text{inf}}} cos\left(\frac{2n\pi}{l}(x - a_{\text{inf}}t)\right)$$
$$U = U_{\text{inf}} + \varepsilon cos\left(\frac{2n\pi}{l}(x - a_{\text{inf}}t)\right)$$
$$\text{for } \frac{l}{2} < x < \frac{l}{2}; t > 0$$

where ρ, U, a, n, l, and ε are respectively the density, velocity, speed of sound, number of waves, length of the domain, and an amplification factor. The speed of sound is equal to $\sqrt{\gamma p/\rho}$ with γ=1.4. The values with a subscript inf are mean values of the flow variables. For this test case p_{inf}=1, ρ_{inf}=γ, ε=10^{-2}, n=1, and l=2. The run time was equal to $4.25\frac{l}{a_{\text{inf}}}$ which allows the wave to propagate through the domain 4.25 times. The CFL number is constant throughout the domain and is equal to 0.75. As seen in Fig. (3) our desired order of convergence closely matches the actual order of convergence. Table (1) shows the desired order of convergence, the actual order of convergence, and the normalized time. The relative numerical cost was calculated by taking the average simulation time per cell per iteration for multiple resolutions and dividing it by the cost of the 2nd order version. The computational scaling shows that by doubling the order of the Taylor series the time required to complete a simulation will increase by about $2^{2.2}$.

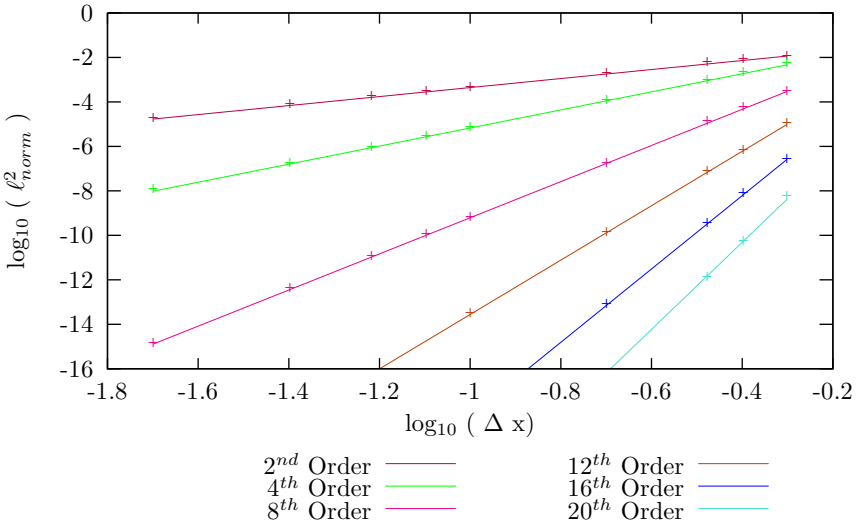

Fig. 3: The ℓ^2 norm of numerical solutions where points are actual calculated data and the line is a best-fit cure of the data.

Desired Order	Actual Order	Normalized Time
2	2.03	1.00
4	4.06	3.43
8	8.12	14.47
12	12.21	34.33
16	16.48	67.98
20	20.52	116.89

Table 1: Convergence rates for the linear acoustic solver and the average normalized time for case.

The above cases showed that we were able to achieve higher-order convergence for coupled, linear, wave equations. In the following, we show fourth-order convergence for solving non-linear equations but for linear physics . The same analytical solution used for the linear acoustic equation is used. There are some problems

when using this solution because the Euler solver will capture the non-linearities present in the flow field while the "analytical" solution does not. This will lead to increasing errors in the analytical solution as Δx decreases. To mitigate the error, the perturbation was reduced to 10^{-6}. For this test case p_{inf}=$1/\gamma$, ρ_{inf}=1, n=2, and l=4 and the simulation time is $2.5\frac{l}{a_{\text{inf}}}$. The CFL number is almost constant throughout the domain and is equivalent to 0.8. As seen in Fig. (4) we achieved a convergence rate of 2.01 and 3.97 for the second- and fourth-order CESE schemes, respectively.

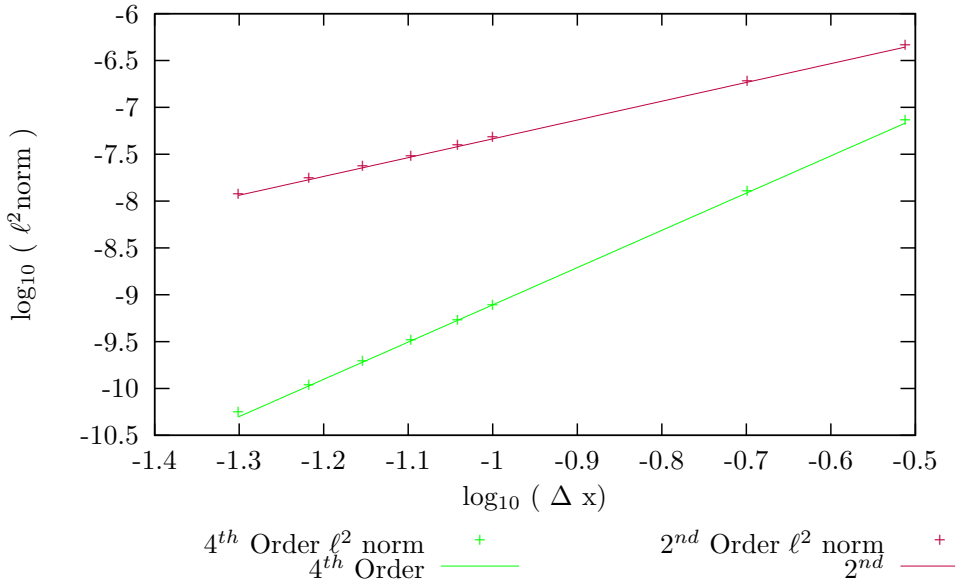

Fig. 4: The ℓ^2 norm of the numerical solutions of the Euler solver for solving the acoustic waves.

The final test case is solving the convection equation with a source term. Under the periodic boundary condition, the analytical solution to this problem is

$$u(x,t) = cos(x-at) + S_0 sin(x),$$
$$-2\pi < x < 2\pi; t > 0.$$

For the convergence tests, $a = S_0 = 1$ and the test time was set to $2.5\frac{l}{a}$, where l is the length of the domain. In all calculations, CFL = 0.7. Shown in Fig. (5) and Table (2), the actual convergence rate agrees well with the order of accuracy of the scheme employed. The computational scaling shows that by doubling the order of the Taylor series the time required to complete a simulation will increase by about $2^{2.2}$.

Desired Order	Actual Order	Normalized Time
2	2.00	1.00
4	4.01	5.22
8	7.95	23.65
12	12.12	59.04
16	16.05	115.83
20	20.09	190.95

Table 2: Convergence rates of the numerical solutions of the convection equation, and the averaged, normalized time for case with different order of accuracy.

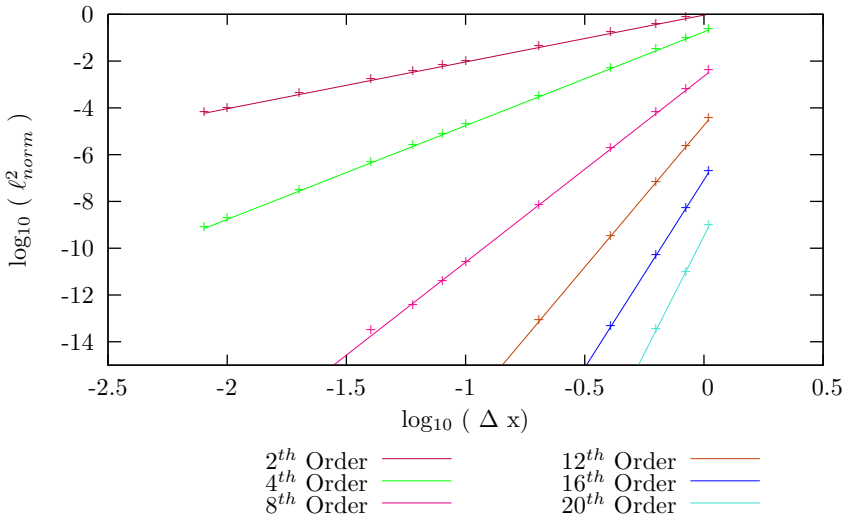

Fig. 5: The ℓ^2 norm of numerical solutions of the Convection equation with source term. The symbols represent the actual calculated data and the lines represent the best-fit curves of the data.

Another important aspect to consider is whether the higher-order resolution is worthy for the additional computational cost. For this, we refer to Figures (6) and (7). Shown in the figures, it is more efficient to use a higher-order method rather than increasing the resolution for a linear solver.

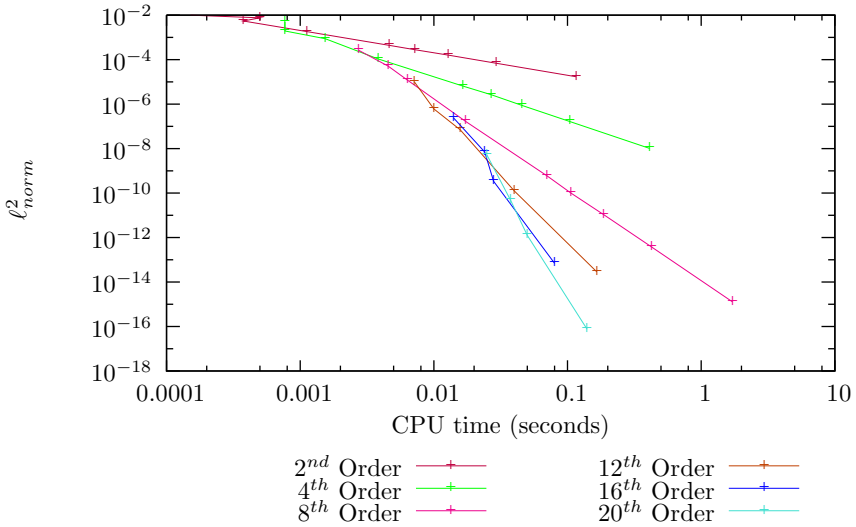

Fig. 6: The ℓ^2 norm versus the computational time for the solutions of the linear acoustic wave equations.

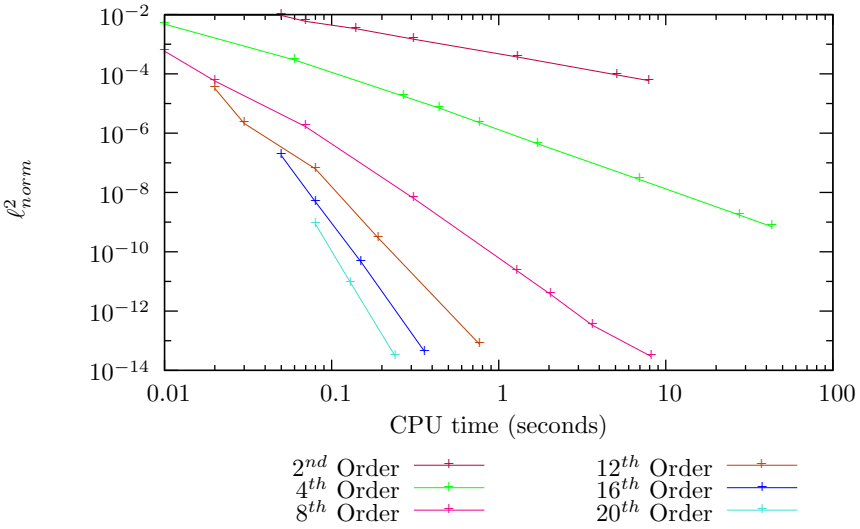

Fig. 7: The ℓ^2 norm versus the computational time for the solution of the convection equation.

Next, we demonstrate the new high-order CESE method by examining numerical resolution for shocks and contact discontinuities. We will run two different test cases at various resolutions and compare the results with an "analytical" results obtained by using very fine mesh. Three solvers will be used in the test cases, the second- and the fourth-order CESE and the fifth- order space third-order time monotonicity preserving (MP53) method.[4] The comparison between the 4^{th}-order CESE scheme and the MP53 method is not completely valid because the CESE scheme employed has higher order in time but low order in space. The test cases chosen are Woodward's blast wave problem and Shu and Osher's problem. Woodward's blast wave problem[5] consists of two shock waves of different strengths heading towards each other with wall boundary conditions. The initial conditions are

$$(u,\rho,p) = \begin{cases} (0, \quad 1, \quad 10^3) & 0 < x < 0.1 \\ (0, \quad 1, \quad 10^{-2}) & 0.1 < x < 0.9 \\ (0, \quad 1, \quad 10^2) & 0.9 < x < 1.0 \end{cases}$$
$$0.0 < t < 0.038.$$

The second test case is Shu and Osher's problem,[6] in which a Mach 3 shock moves to the right and collides with an entropy disturbance moving to the left. The boundary conditions are non-reflective and the initial conditions are

$$(u,\rho,p) = \begin{cases} (2.629369, \quad 3.857143, \quad 10.3333) & -1 < x < -0.8 \\ (0, \quad 1 + 0.2\sin(5\pi x), \quad 1) & -0.8 < x < 1.0 \end{cases}$$
$$0.0 < t < 0.47.$$

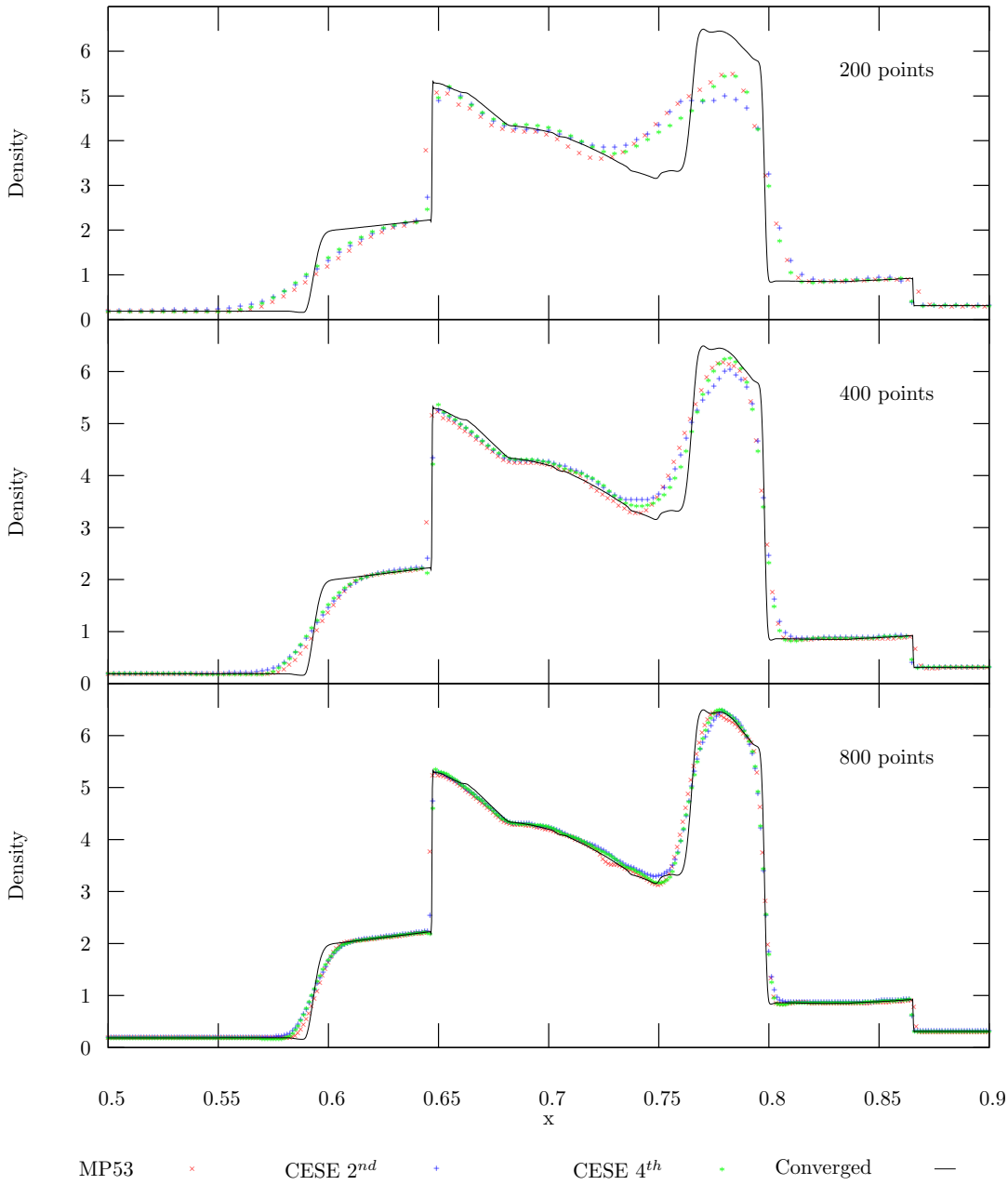

Fig. 8: Plots of the density profiles of the Woodwards blast wave problem. The converged simulation was done by using the fourth-order CESE with 3201 points. For better presentation, only a subset of the domain is shown in these plots.

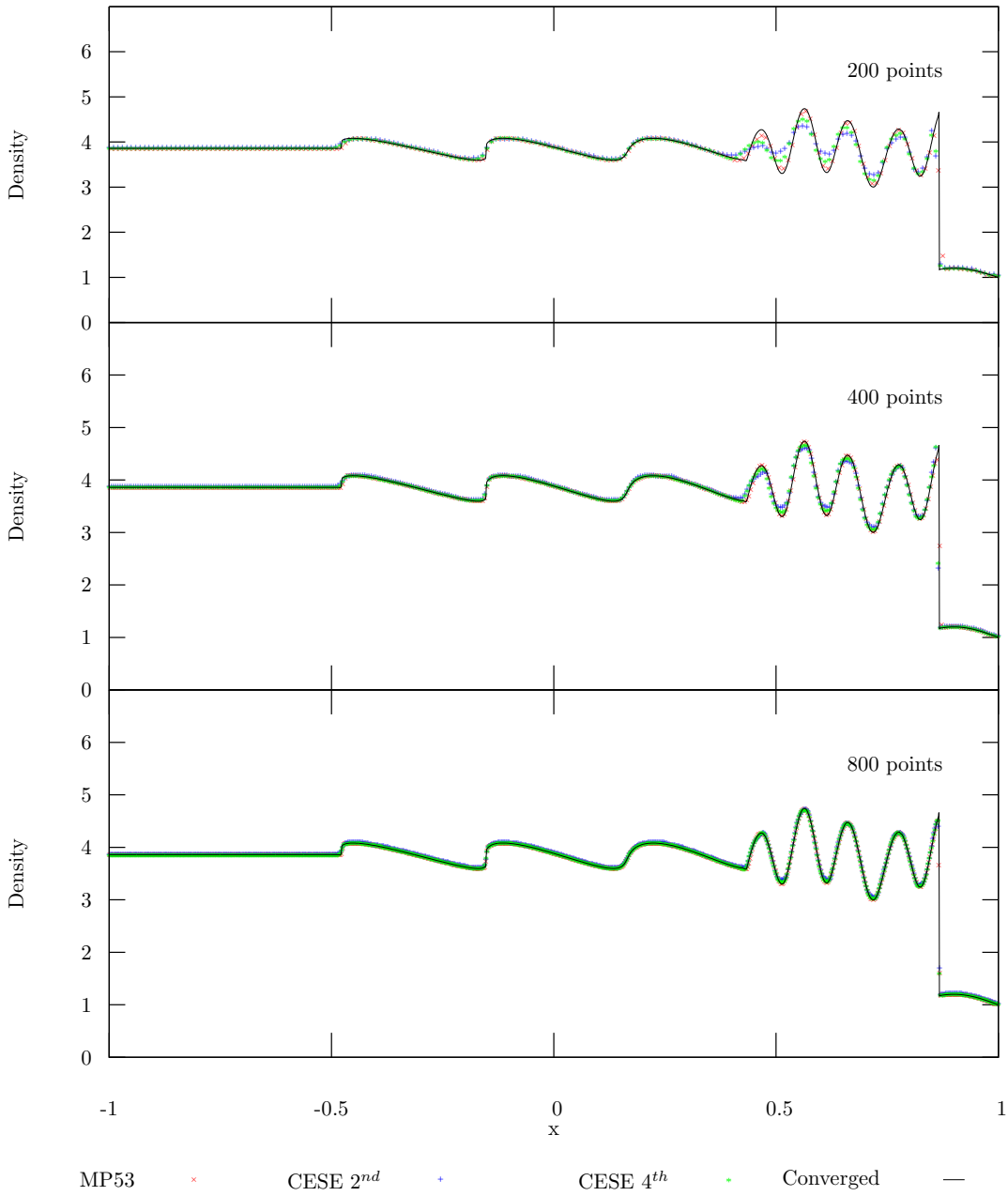

Fig. 9: Plots of the calculated density profiles for Shu and Osher's problem. Each plot has a different spatial resolution. The converged simulation was done by using the fourth-order CESE scheme with 3201 points.

For both simulations using the second- and fourth-order CESE methods, α in Eq. (20) is set to be unity. Shown in Figures (8) and (9), the fourth-order CESE method provides more accurate solutions than the second-order CESE method in the region where the solution is smooth. When discontinuities are present, the fourth-order scheme still does a better job but has more overshoots than the second-order CESE method. Moreover, the results obtained by using CESE schemes compare favorably with that by the MP53 scheme.

V. Concluding Remarks

In this paper, we extended Chang's fourth-order CESE method for one convection equation for solving a system of coupled hyperbolic PDE's with arbitrarily high-order convergence. Numerical results show that

the extended algorithm can achieve higher-order convergence for both linear and non-linear hyperbolic PDEs. The shock-capturing capability of the new method was comparable to that of the original second-order CESE scheme as well as that of the fifth-order space third-order time monotonicity preserving scheme. Further development of the high-order CESE method can benefited from investigations in several areas, including the effect of different limiters on the higher-order derivatives, and the effects of the boundary condition treatments and the source-term treatments for high-order accuracy.

VI. Acknowledgments

The authors would like to thank Lord Cole for the MP53 solutions to Woodward's blast wave problem and Shu and Osher's test case.

References

[1]Chang, S., "A New Approach for Constructing Highly Stable High Order CESE Schemes," AIAA-2010-543, 48th AIAA Aerospace Science Meeting, Orlando, FL, Jan. 2010.

[2]Chang, S., "The Method of Space-Time Conservation Element and Solution Element – A New Approach for Solving the Navier-Stokes and Euler Equations," *Journal of Computational Physics*, Vol. 119, No. 2, July 1995, pp. 295–324.

[3]Chang, S. and Wang, X., "Multi-Dimensional Courant Number Insensitive CE/SE Euler Solvers for Applications Involving Highly Nonuniform Meshes," *39th AIAA/ASME/SAE/ASEE Joint Propulsion Conference and Exhibit*, Huntsville, Alabama, July 2003.

[4]Suresh, A. and Huynh, H. T., "Accurate Monotonicity-Preserving Schemes with Runge-Kutta Time Stepping," *Journal of Computational Physics*, Vol. 136, No. 1, Sept. 1997, pp. 83–99.

[5]Woodward, P. and Colella, P., "The numerical simulation of two-dimensional fluid flow with strong shocks," *Journal of Computational Physics*, Vol. 54, 1984, pp. 115–173.

[6]Shu, C. and Osher, S., "Efficient implementation of essentially non-oscillatory shock capturing schemes II," *Journal of Computational Physics*, Vol. 83, 1989, pp. 32–78.